JACS
JOURNAL OF THE AMERICAN CHEMICAL SOCIETY

Article

pubs.acs.org/JACS

Molecular Engineering of Mechanochromic Materials by Programmed C−H Arylation: Making a Counterpoint in the Chromism Trend

Jie Wu,[†,§] Yangyang Cheng,[†,§] Jingbo Lan,[*,†] Di Wu,[†] Shengyou Qian,[†] Lipeng Yan,[†] Zhen He,[†] Xiaoyu Li,[†] Kai Wang,[‡] Bo Zou,[*,‡] and Jingsong You[*,†]

[†]Key Laboratory of Green Chemistry and Technology of Ministry of Education, College of Chemistry, and State Key Laboratory of Biotherapy, West China Medical School, Sichuan University, 29 Wangjiang Road, Chengdu 610064, P.R. China

[‡]State Key Laboratory of Superhard Materials, Jilin University, Changchun 130012, P.R. China

Supporting Information

ABSTRACT: The development of facile methods for screening organic functional molecules through C−H bond activation is a revolutionary trend in materials research. The prediction of mechanochromism as well as mechanochromic trends of luminogens is an appealing yet challenging puzzle. Here, we present a strategy for the design of mechanochromic luminogens based on the dipole moment of donor−acceptor molecules. For this purpose, a highly efficient route to 2,7-diaryl-[1,2,4]triazolo[1,5-*a*]pyrimidines (2,7-diaryl-TAPs) has been established through programmed C−H arylation, which unlocks a great opportunity to rapidly assemble a library of fluorophores for the discovery of mechanochromic regularity. Molecular dipole moment can be employed to explain and further predict the mechanochromic trends. The 2,7-diaryl-TAPs with electron-donating groups on the 2-aryl and electron-withdrawing groups on the 7-aryl possess a relatively small dipole moment and exhibit a red-shifted mechanochromism. When the two aryls are interchanged, the resulting luminogens have a relatively large dipole moment and display a blue-shifted mechanochromism. Seven pairs of isomers with opposite mechanochromic trends are presented as illustrative examples. The aryl-interchanged congeners with a bidirectional emission shift are structurally similar, which provides an avenue for understanding in-depth the mechanochromic mechanism.

INTRODUCTION

Mechanochromic materials sensitive to mechanical stimuli have attracted extensive interest due to their promising applications in mechanical sensors, deformation detectors, security systems, and memory devices.[1−18] Mechanochromism of organic conjugated materials greatly depends on molecular packing associated with intermolecular interactions such as $\pi-\pi$, hydrogen bond, and dipole−dipole interactions.[19−21] Owing to the inherent intricacies of molecular structural factors and intermolecular forces, it seems difficult to predict the mechanochromic behavior of chromophores. Therefore, it is also greatly challenging to achieve a major breakthrough in the rational molecular design of mechanochromic materials.[21] To date, organic small-molecule materials with mechanochromic properties are still limited and have often appeared as a single isolated event.[1,21] Molecular engineering is an important part of pharmaceutical research and materials science. The establishment of a rapid gateway toward a large library of fluorescent molecules will doubtlessly unlock a golden opportunity to gain a better understanding of the structure−property relationships of mechanochromic materials.

In this article, we demonstrate a novel strategy for the design of mechanochromic luminogens based on the dipole moment of donor−acceptor (D-A) molecules. We also hope to exemplify the important role of C−H bond activation in the lead-optimization phase of developing organic functional materials. Molecular engineering, established herein through the programmed C−H arylation of heteroaromatics, provides an opportunity to rapidly assemble a library of D-A-type luminogens and further discover mechanochromic regularity.

RESULTS AND DISCUSSION

Molecular Design. The electron-deficient (hetero)-aromatic ring has proven well-suited to give birth to strong $\pi-\pi$ interaction because of its low π-electron density.[22,23] [1,2,4]Triazolo[1,5-*a*]pyrimidine (TAP), fused by pyrimidine and triazole together, is a typical, strongly electron-deficient heteroaromatic ring. Although the emission maximum of TAP is located in the ultraviolet region (389 nm in CH_2Cl_2), the introduction of electron-rich aryl moiety enables a red-shifted

Received: April 15, 2016
Published: September 7, 2016

DOI: 10.1021/jacs.6b03890
J. Am. Chem. Soc. 2016, 138, 12803−12812

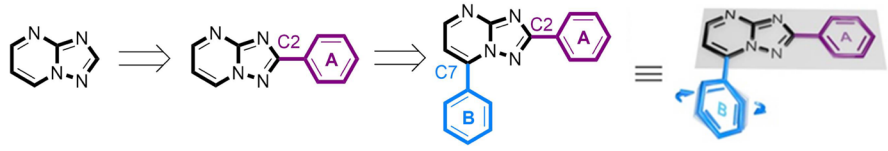

Figure 1. Molecular design of diaryl-TAPs.

emission to visible region through an extended π-conjugation and intramolecular charge transfer (ICT).[24,25] Given that the biaryls consisting of one six-membered ring and one five-membered ring (6:5) usually prefer planar geometries, while the biaryls consisting of two six-membered rings (6:6) favor more twisted conformations than the 6:5 biaryl systems,[26] 2-aryl-TAP (**A-TAP**) with the 6:5 system could adopt a coplanar conformation and 7-aryl-TAP (**B-TAP**) with the 6:6 system could take a twisted structure. Thus, in the absence of a steric hindrance group at the *ortho*-position of the **A** ring, the plane of the **A-TAP** segment of 2,7-diaryl [1,2,4]triazolo[1,5-*a*]-pyrimidines (2,7-diaryl-TAPs) is favorable to the face-to-face $\pi-\pi$ interaction, and the rotation of the **B** ring can modify the molecular planarity and the plane-to-plane spacing. The face-to-face $\pi-\pi$ and dipole−dipole interactions of two adjacent donor−acceptor (D-A) molecules, which place the donor moiety of one molecule above the acceptor moiety of its neighboring molecule,[27] may induce various molecular packing modes. The incorporation of donor/acceptor substituents on the **A** and **B** rings could alter the dipole moment of molecule and the dihedral angle of the **B-TAP** section. A mechano-dependent switching of molecular packing modes could be achieved through the rotation of the **B** ring and the shift of the π-plane to endow a chromism response. Herein, we envision that the 2,7-diaryl-TAP core would be a promising candidate for molecular engineering investigation to assess the relationship between molecular structure and mechanochromic luminescent behavior (Figure 1).

Synthesis and Photophysical Properties of Aryl-TAPs. To test our hypothesis, it is necessary to develop a concise and rapid approach to a library of 2,7-diaryl-TAP molecules. Conventional cyclization reactions to 2-aryl- and 7-aryl-TAPs generally suffer from several limitations such as multistep procedures and/or hardly accessible synthetic precursors,[28−30] which limit the rapid assembly of a structurally diverse chemical library. Transition metal-catalyzed C−X/C−M coupling reactions are reliable approaches to access heteroaryl−aryl structures. We initially tried to perform the bromination at C2-position of TAP. However, the bromination of TAP occurred preferentially at C7 rather than at C2 and gave 7-bromo-substituted TAP as the only product (for details, see section II in Supporting Information (SI)). Thus, the sequential insertion of a halide at C2 of TAP and C−X/C−M cross-coupling reaction is not a viable synthetic route to 2-aryl-TAPs. Subsequently, we explored the direct C2-arylation of TAP to construct 2-aryl-TAPs via a C−H/C−X coupling reaction.[31−33] However, the direct arylation of TAP with 4-iodotoluene occurred at C7 rather than at C2 (Table S1). Although the C7-arylation gave us an opportunity to assemble 2,7-diaryl-TAPs by further C2-arylation of the resulting 7-aryl-TAP, all efforts failed to reach the goal. Thus, we have to pursue other approaches to synthesize 2-aryl-TAPs (Scheme 1).

The Dimroth rearrangement is an isomerization of heterocycles through a ring opening/ring closure sequence, which can enable a transformation from [1,2,4]triazolo[4,3-*a*]pyrimidine

Scheme 1. Programmed C−H Arylation for the Synthesis of 2,7-Diaryl-TAPs

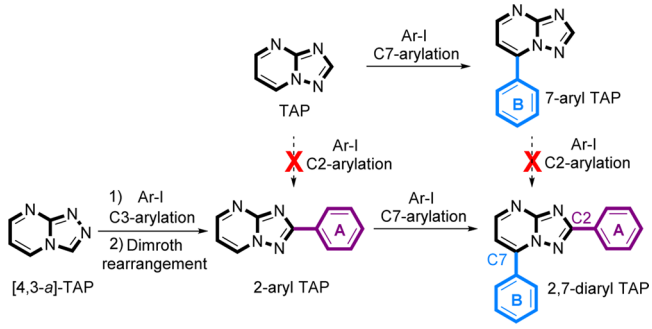

to [1,2,4]triazolo[1,5-*a*]pyrimidine.[29] Thus, it is envisaged that 2-aryl-TAPs (**3**) could be obtained by direct C3−H arylation of [1,2,4]triazolo[4,3-*a*]pyrimidine ([4,3-*a*]-TAP, **1a′**) and subsequent Dimroth rearrangement (Table 1). As expected, the sequential CuI-catalyzed C3-arylation of **1a′** with iodobenzene (**2e**) and Dimroth rearrangement in formic acid successfully delivered the 2-arylated **3e** in 71% yield in a one-pot process (Table S2). The intermediate **3e′** was isolated in the absence of formic acid, and its structure was confirmed by single-crystal X-ray diffraction (Table 1 and Figure S1). To investigate the relationship between structure and photophysical properties,[34−36] a library of 2-aryl-TAPs with various substituents was assembled under the optimal conditions, and their photophysical properties are shown in Table 1. It is found that the introduction of an electron-donating group (EDG) on the **A** ring results in a red-shifted emission (Table 1, **3a−3d** and **3j**), while an electron-withdrawing group (EWG) has little influence on emission (Table 1, **3f−3i**). As we expected, the crystallography data of **3d** exhibit an almost planar conformation of **A**-TAP (a dihedral angle of only 5.6°) (Table 1).

Subsequently, we focused on the synthesis of 7-aryl-TAPs. After screening several reaction parameters (for details, see Table S1), a library of 7-aryl-TAPs was assembled in 1,4-dioxane using K_3PO_4 as the base and pivalic acid as the additive in the presence of CuI/1,10-phenanthroline. The crystal structure of **4a** reveals a 27.8° dihedral angle between 7-tolyl and TAP, demonstrating a twisted conformation of **B-TAP**. The spectral data of 7-aryl-TAPs are collected in Table 2. All 7-aryl-TAPs exhibit a short-wavelength emission of around 400 nm except **4d** (Table 2).

To evaluate the electronic effect of substituents on the **A** and **B** rings, the highest occupied molecular orbital (HOMO) and lowest unoccupied molecular orbital (LUMO) distributions and energy levels of both 2-aryl- and 7-aryl-TAPs were calculated by the density functional theory (DFT) (for details, see section IV in SI).[37] Compared with 2-phenyl-TAP (**3e**), an EDG on the **A** ring has little influence on the LUMO level, but significantly pushes the HOMO level up, hence narrowing the bandgaps of 2-aryl-TAPs (**3a**, **3b**, **3c**, **3d**, and **3j**). Compared with 7-phenyl-TAP (**4e**), an EDG on the **B** ring also reduces

DOI: 10.1021/jacs.6b03890
J. Am. Chem. Soc. 2016, 138, 12803−12812

Table 1. One-Pot Synthesis and Photophysical Properties of 2-Aryl-TAPs[a]

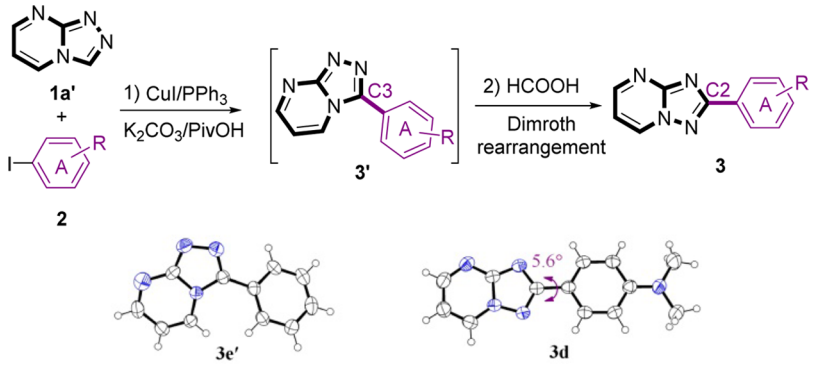

compd	A ring	yield[b] (%)	λ_{abs}[c] (nm)	λ_{em}[c] (nm) (Φ_f[d])	Stokes shift (cm^{-1})
3a	4-CH_3Ph	61	310	392 (0.67)	6748 (82 nm)
3b	4-CH_3OPh	73	317	402 (0.57)	6670 (85 nm)
3c	3,4-$(CH_3O)_2$Ph	38	325	452 (0.81)	8645 (127 nm)
3d	4-$(CH_3)_2$NPh	10	358	519 (0.52)	8665 (161 nm)
3e	Ph	71	304	356 (0.86)	4805 (52 nm)
3f	3,5-$(CF_3)_2$Ph	50	294	351 (0.05)	5524 (57 nm)
3g	4-ClPh	77	305	358 (0.32)	4854 (53 nm)
3h	4-CHOPh	79	305	358 (0.19)	4854 (53 nm)
3i	4-CNPh	52	296	356 (0.29)	5694 (60 nm)
3j[e]	4-piperidylPh	45	349	527 (0.32)	9678 (178 nm)

[a]Reaction conditions: 1) **1a′** (0.25 mmol), **2** (0.375 mmol), CuI (10 mol %), PPh_3 (10 mol %), PivOH (50 mol %), K_2CO_3 (2.0 equiv), and 1,4-dioxane/DMSO (0.6/0.06 mL) at 120 °C for 24 h under N_2. 2) HCOOH (1.0 mL) at 110 °C for 12 h. PivOH = pivalic acid; DMSO = dimethyl sulfoxide. [b]Isolated yield. [c]Absorption maximum and emission maximum in CH_2Cl_2 (10 μM). [d]Absolute quantum yield in CH_2Cl_2 (10 μM) was determined with an integrating sphere system. [e]For the synthetic details of **3j**, see section VIII in SI. Inset: X-ray crystal structures of **3e′** and **3d** with thermal ellipsoids at 50% probability.

Table 2. Synthesis and Photophysical Properties of 7-Aryl-TAPs[a]

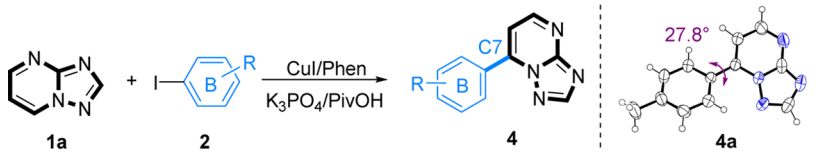

compd	B ring	yield[b] (%)	λ_{abs}[c] (nm)	λ_{em}[c] (nm) (Φ_f[d])	Stokes shift (cm^{-1})
4a	4-CH_3Ph	90	312	384 (0.88)	6010 (72 nm)
4b	4-CH_3OPh	73	326	389 (0.85)	4968 (63 nm)
4c	3,4-$(CH_3O)_2$Ph	67	339	411 (0.75)	5168 (72 nm)
4d	4-$(CH_3)_2$NPh	62	389	449 (0.99)	3435 (60 nm)
4e	Ph	86	310	374 (0.70)	5520 (64 nm)
4f	3,5-$(CF_3)_2$Ph	79	296	399 (0.99)	8721 (103 nm)
4g	4-ClPh	77	309	394 (0.80)	6982 (85 nm)
4h	4-CHOPh	74	309	390 (0.85)	6721 (81 nm)
4i	4-CNPh	52	300	400 (0.51)	8333 (100 nm)
4j	4-piperidylPh	42	387	460 (0.98)	4101 (73 nm)

[a]Reaction conditions: **1a** (0.25 mmol), **2** (0.375 mmol), CuI (10 mol %), Phen (10 mol %), PivOH (50 mol %), K_3PO_4 (2.0 equiv), and 1,4-dioxane (0.6 mL) at 140 °C for 24 h under N_2. Phen = 1,10-phenanthroline. [b]Isolated yield. [c]Absorption maximum and emission maximum in CH_2Cl_2 (10 μM). [d]Absolute quantum yield in CH_2Cl_2 (10 μM) was determined with an integrating sphere system. Far right inset: X-ray crystal structure of **4a** with thermal ellipsoids at 50% probability.

the bandgaps of 7-aryl-TAPs (**4a**, **4b**, **4c**, **4d**, and **4j**), but its influence is smaller than that on 2-aryl-TAPs. On the other hand, an EWG on the **A** ring almost synchronously reduces both the HOMO and LUMO levels, and thus the bandgaps of 2-aryl-TAPs remain almost unchanged in comparison with **3e**. In contrast, compared with **4e**, an EWG on the **B** ring causes a larger decrease of the LUMO level than that of the HOMO level (**4f**, **4g**, **4h**, and **4i**). Thus, the bandgap is reduced more efficiently by an EWG on the **B** ring than on the **A** ring. In addition, we also chart the scatter plot of emission wavelengths versus Hammett constants (Figure 2).[38] These observations illustrate that an EDG on the **A** ring can cause a more red-shifted emission than on the **B** ring, while an EWG on the **B** ring can induce a larger red-shift than on the **A** ring. Thus, we rationalize that an EDG on the **A** ring and an EWG on the **B** ring would lead to a much more red-shifted emission.

DOI: 10.1021/jacs.6b03890
J. Am. Chem. Soc. 2016, 138, 12803−12812

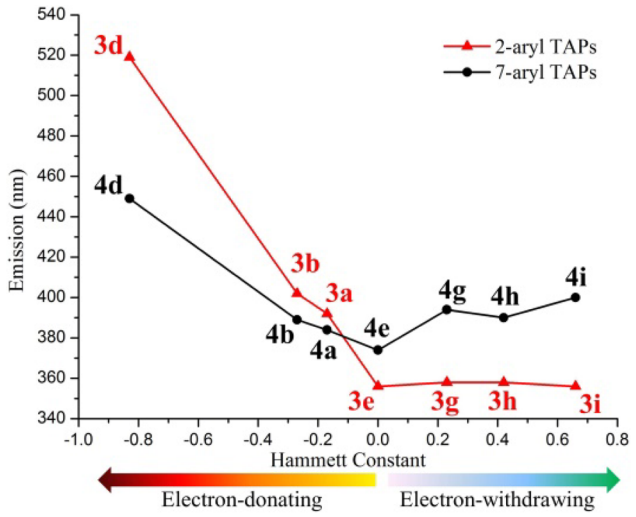

Figure 2. Electronic effect of substituents on the **A** and **B** rings. The scatter plot of the emission maxima of C2- and C7-aryl-TAPs versus Hammett constants is charted.

As C2-arylation and C7-arylation of TAP proceed independently, 2,7-diaryl-TAPs are easily constructed by using the programmed C3−H arylation, Dimroth rearrangement, and C7−H arylation. Thus, a series of 2,7-diaryl-TAPs with different substituents on the **A** and **B** rings were synthesized in satisfactory yields. Photophysical data of these fluorophores both in solution and in the solid state are summarized in Table 3 (for details, see Table S3 and Figure S4). As expected, 2,7-diaryl-TAPs with EDG on the **A** ring and EWG on the **B** ring (**5ji**, **5di**, **5df**, **5dg**, and **5af**) exhibit a more red-shifted emission in solution compared with 2,7-diphenyl-TAP (**5ee**). It needs to note that **5df** shows a significant red shift of emission in CH_2Cl_2 (λ_{em} = 620 nm) compared to its solid state (λ_{em} = 539 nm), while its aryl-interchanged congener **5fd** displays a remarkable blue shift of emission in CH_2Cl_2 (λ_{em} = 462 nm) compared to its solid state (λ_{em} = 620 nm). To get insight into the difference in their emissions between in solution and in the solid state, the solvatochromic effects[39] and fluorescence spectra at different concentrations of **5df** and **5fd** were investigated (for details, see section V in SI). The dipole moment changes ($\Delta\mu = \mu_e - \mu_g$) between the fluorescent excited state and ground state were calculated to be 15.76 and 7.85 D for **5df** and **5fd**, respectively. The much larger $\Delta\mu$ value of **5df** indicates a more significant ICT effect than **5fd**. To further confirm the ICT effect, **5df** was subjected to the density functional theory (DFT) calculation at B3LYP/6-31G(d) level. The HOMO is primarily localized over the *N*,*N*-dimethylamino-substituted phenyl moiety (**A** ring), while the LUMO is mainly centered on the 3,5-ditrifluoromethyl-substituted phenyl moiety (**B** ring) (Figure S14). Both the large value of $\Delta\mu$ and the DFT calculation suggest that **5df** is a typical D-A type molecule with significant ICT effect.[40] In addition, the emission spectrum of **5df** powder (Figure S8) is similar to that of its dilute solution in low polar solvent (Figure S5), and no concentration-dependent emission spectrum was observed (1×10^{-5} to 1×10^{-2} M) (Figure S7), which excludes the excimer formation.[41] Therefore, a significant emission red shift of **5df** in solution compared to its solid state may be mainly attributed to a significant ICT effect. In contrast, **5fd** exhibits a relatively small ICT effect due to the small $\Delta\mu$ value. An obvious concentration-dependent emission spectrum at approximately 595 nm is observed for **5fd** (1×10^{-5} to 1×10^{-2} M) (Figure S7), which is similar to its solid spectrum (Figure S8), indicating the excimer formation.[42] These observations demonstrate that the remarkable emission red shift of **5fd** in

Table 3. Synthesis and Photophysical Properties of 2,7-Diaryl-TAPs[a]

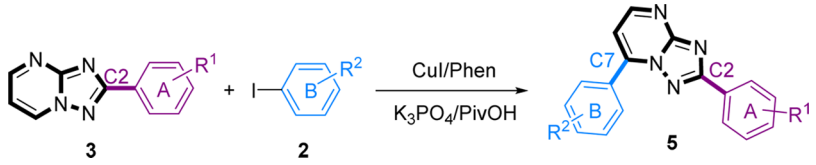

3 2 5

compd	A ring	B ring	yield[b] (%)	λ_{abs}[c] (nm)	λ_{em}[c] (nm) (Φ_f[d])	Stokes shift (cm^{-1})	λ_{em}[e] (nm)
5ji	4-piperidylPh	4-CNPh	64	391	653 (0.01)	10262 (262 nm)	574
5di	4-$(CH_3)_2$NPh	4-CNPh	61	400	645 (0.01)	9496 (245 nm)	615
5df	4-$(CH_3)_2$NPh	3,5-$(CF_3)_2$Ph	69	402	620 (0.02)	8747 (218 nm)	539
5dg	4-$(CH_3)_2$NPh	4-ClPh	67	378	573 (0.38)	9003 (195 nm)	522
5da	4-$(CH_3)_2$NPh	4-CH_3Ph	87	373	553 (0.33)	8726 (180 nm)	515
5ef	Ph	3,5-$(CF_3)_2$Ph	88	318	401 (0.42)	6509 (83 nm)	409
5af	4-CH_3Ph	3,5-$(CF_3)_2$Ph	79	324	420 (0.61)	7055 (96 nm)	414
5aa	4-CH_3Ph	4-CH_3Ph	82	317	390 (0.62)	5905 (73 nm)	398
5ee	Ph	Ph	88	317	389 (0.25)	5839 (72 nm)	405
5fa	3,5-$(CF_3)_2$Ph	4-CH_3Ph	79	309	379 (0.64)	5977 (70 nm)	404
5fe	3,5-$(CF_3)_2$Ph	Ph	78	305	389 (0.95)	7080 (84 nm)	407
5ad	4-CH_3Ph	4-$(CH_3)_2$NPh	78	391	450 (0.99)	3353 (59 nm)	539
5gd	4-ClPh	4-$(CH_3)_2$NPh	61	394	453 (0.86)	3306 (59 nm)	610
5fd	3,5-$(CF_3)_2$Ph	4-$(CH_3)_2$NPh	75	401	462 (0.80)	3293 (61 nm)	620
5id	4-CNPh	4-$(CH_3)_2$NPh	47	402	464 (0.96)	3324 (62 nm)	584
5ij	4-CNPh	4-piperidylPh	62	400	473 (0.98)	3858 (73 nm)	567

[a]Reaction conditions: **3** (0.25 mmol), **2** (0.375 mmol), CuI (10 mol %), Phen (10 mol %), PivOH (50 mol %), K_3PO_4 (2.0 equiv), and 1,4-dioxane (0.6 mL) at 140 °C for 24 h under N_2. [b]Isolated yield. [c]Absorption maximum and emission maximum in CH_2Cl_2 (10 μM). [d]Absolute quantum yield in CH_2Cl_2 (10 μM) was determined with an integrating sphere system. [e]Emission maximum in pristine powder.

DOI: 10.1021/jacs.6b03890
J. Am. Chem. Soc. 2016, 138, 12803−12812

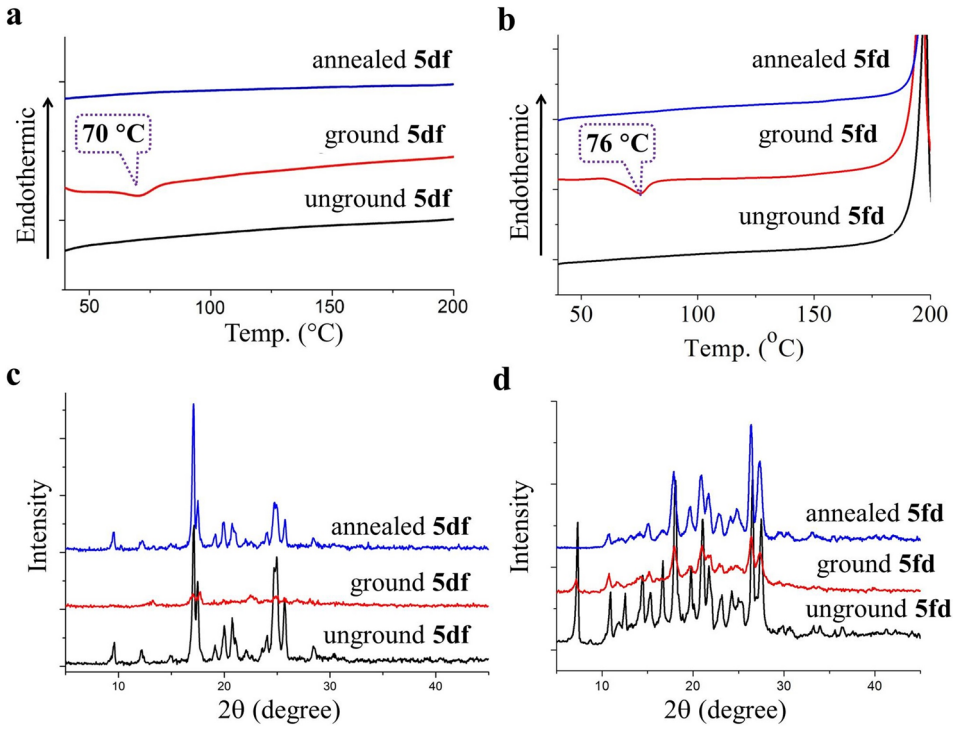

Figure 3. DSC curves of **5df** (a) and **5fd** (b) in different states. XRD patterns of **5df** (c) and **5fd** (d) in different states.

the solid state compared to its solution may be mainly attributed to the excimer formation.

Relationship between Molecular Structure and Mechanochromic Luminescent Behavior. With 2,7-diaryl-TAPs in hand, we evaluated the mechanochromic behaviors of these luminogens. The chromophores exhibit solid-state fluorescence covering the entire visible region (404−620 nm) (Table 3). Upon grinding, except 2,7-ditolyl-TAP (**5aa**) and 2,7-diphenyl-TAP (**5ee**), these molecules exhibit mechanochromic behaviors (Table S3 and Figure S8). Among them, **5ji**, **5di**, **5df**, **5dg**, **5da**, **5ef**, and **5af** show red-shifted mechanochromic luminescence properties. In contrast, their aryl-interchanged isomers, **5ij**, **5id**, **5fd**, **5gd**, **5ad**, **5fe**, and **5fa**, exhibit blue-shifted mechanochromic behaviors (see Figure 5, below). These results indicate that the exchange between the C2-aryl and C7-aryl moieties does make a counterpoint in chromism trends.

Taking **5df** and **5fd** as representative examples, the mechanofluorochromic behaviors were investigated in details. Grinding of the pristine powder **5df** induced a substantial red-shift with an emission color change from yellowish-green (λ_{em} = 539 nm) to orange-red (λ_{em} = 588 nm) (see Figure 5). In contrast, the original powder of **5fd** shows a red emission with an emission maximum of 620 nm. Upon grinding, the emission color blue-shifts to orange-yellow (λ_{em} = 563 nm). These observations indicate that the luminogens **5df** and **5fd** with the interchanged **A** and **B** rings exhibit an opposite mechanochromic trend. Differential scanning calorimetry (DSC) analyses for the different states of **5df** and **5fd** show that the ground samples present an obvious exothermal peak at approximately 70 and 76 °C, respectively, indicating a phase transition between the metastable ground state and the more stable original state or annealing state (Figure 3a,b). The emission of **5df** could be reversibly switched between different states by repeated grinding and annealing treatments with no obvious fatigue response (Figure S9). Moreover, the emission of ground **5df** could also be restored by solvent fuming in a wide range of solvent vapors for 1−3 min (Table S5). It needs to point out that the emission of ground **5fd** could only be restored to 582 nm by annealing.

To gain an in-depth understanding of structure−property relationship of these mechanochromic materials, the analysis of powder X-ray diffraction (PXRD) of the pristine, ground, and annealed **5df** and **5fd** was conducted (Figure 3c,d). The PXRD patterns of the original powders exhibit sharp and intense reflection peaks, but these sharp peaks almost disappear after grinding treatment. These observations demonstrate a morphological transition between the crystalline (ordered) and amorphous (disordered) phases. Upon thermal annealing of ground **5df** and **5fd** at 120 °C for 10 min, the sharp peaks in the PXRD patterns could be recovered. In addition, the changes of UV−visible absorption spectra of the pristine and ground **5df** and **5fd** also manifest an evident change of the packing mode upon grinding (Figure S10).

By slowly evaporating EtOAc or CH_3CN solution of **5df** and **5fd**, the single crystals were obtained. The crystals of **5df** exhibit yellowish-green fluorescence with an emission maximum of 524 nm (Figure 4a). By grinding the crystals, the emission color red-shifts to orange-red (λ_{em} = 588 nm). Single-crystal XRD analysis of **5df** reveals the face-to-face antiparallel packing between the two adjacent 2-aryl-TAP planes (Figure 4b). The electron-poor TAP moiety of one molecule is located above the electron-rich 4-dimethylaminophenyl moiety of its neighboring molecule. The TAP core frameworks form columnar stacked array along the *a* axis, in which the stacked molecules alternately take the opposite direction with the intermolecular distances of 3.87 and 3.52 Å, indicating relatively weak $\pi-\pi$ interactions between the 2-aryl-TAP planes. In each molecule, the **A** ring is nearly coplanar with the central TAP moiety with a negligible dihedral angle of 1.0°, which is

DOI: 10.1021/jacs.6b03890
J. Am. Chem. Soc. 2016, 138, 12803−12812

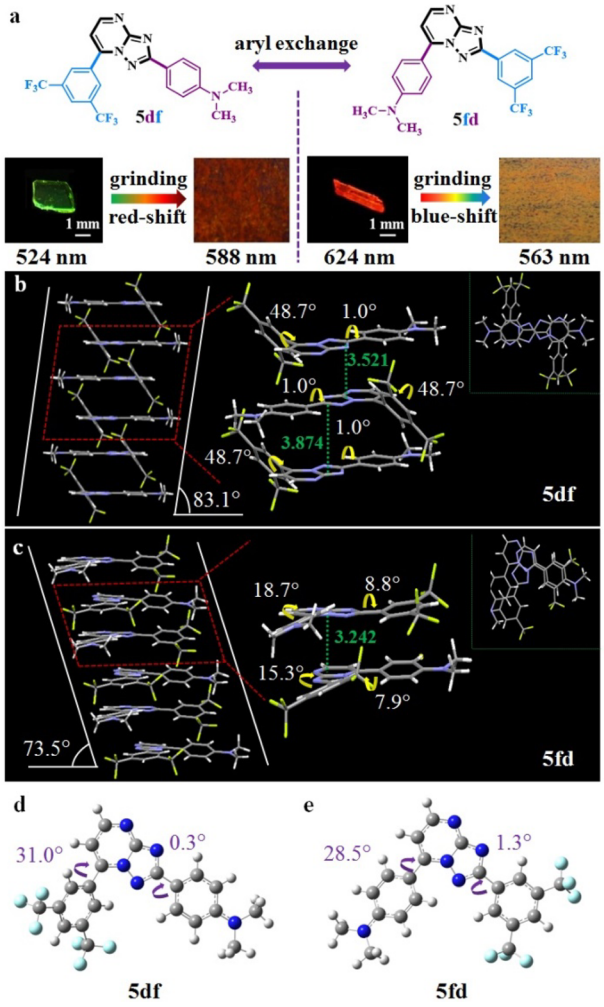

Figure 4. (a) Photographs of single crystals and ground samples of **5df** and **5fd** under UV light (365 nm). (b) Antiparallel packing mode of crystal **5df**. (c) Cross-parallel packing mode of crystal **5fd**. The top view of the crystalline packing is shown in upper right corner. Calculated molecular conformations of **5df** (d) and **5fd** (e).

indicative of a perfect π-conjugation in the 2-(4-dimethylaminophenyl)-TAP section. The **B** ring twists out of the **A-TAP** plane with a large dihedral angle of 48.7°. DFT calculation of the isolated molecule of **5df** discloses a twisting angle of 31.0° between the **B** ring and the **A-TAP** plane, which is smaller than that in the crystalline state (Figure 4d). The fluorophore takes a more distorted configuration to fit into the crystalline lattice. Once the crystalline lattice is broken upon grinding, the originally twisted segments may relax to become more planar. It means that the **B** ring may rotate from 48.7° to a smaller dihedral angle and finally approach 31.0° when external pressure breaks the bondage of partial lattice energy.[43] Thus, the π-conjugation degree as well as intermolecular $\pi-\pi$ interactions are enhanced, thus leading to a red-shifted emission.[10]

While the **A** and **B** rings of **5df** are interchanged, the crystal structure of the resulting **5fd** displays an unusual cross-parallel packing mode, in which the electron-deficient 3,5-bis(trifluoromethyl)phenyl moiety of one molecule and the electron-rich 4-dimethylaminophenyl moiety of another molecule are oriented nearly parallel to each other, and the TAP cores of two different molecules are arranged in a cross-orientation (Figure 4c). Different from **5df**, the twisting angle between the **B** ring and the TAP moiety of **5fd** is decreased dramatically, which leads to a roughly coplanar arrangement of molecules. Each repeating unit of the crystal structure is composed of two molecules with different dihedral angles (8.8° and 18.7° for one unit, and 7.9° and 15.3° for another). A vertical distance between two 2-aryl-TAP planes is measured to be approximately 3.24 Å, indicating a strong $\pi-\pi$ interaction. The crystals of **5fd** exhibit a red fluorescence (λ_{em} = 624 nm) with a weak emission (Φ_f < 0.01) due to the close face-to-face stacking, which is consistent with the excimer character.[44] Upon grinding, the emission color blue-shifts to yellow (λ_{em} = 563 nm), with an enhanced emission efficiency (Φ_f = 0.04) and a shortened lifetime (from 7 to 4 ns) (Figure S11), implying a diminished excimer formation. Thus, the fluorescence blue shift after grinding crystals can be ascribed to the weakened intermolecular $\pi-\pi$ interactions. In addition, DFT calculation of the isolated molecule of **5fd** indicates that the **A-TAP** section adopts a planar conformation with a dihedral angle of 1.3° and the **B** ring adopts a twisted geometry with a dihedral angle of 28.5° (Figure 4e). The twisted **B** ring is probably ascribed to the steric repulsion between two aryl *ortho* hydrogen atoms of the 6:6 biaryl structure.[26] It is conceived that a great torsional tension existing in the molecule of the crystalline state may be balanced with the intermolecular face-to-face $\pi-\pi$ and dipole–dipole interactions. The mechanical force enables to break such a balance and further induce more twisted conformations, which weakens intramolecular π-conjugation and intermolecular $\pi-\pi$ stacking interactions to induce a blue-shifted emission.

To gain further insight into the opposite mechanochromic shifts for these aryl-interchanged isomers, the dipole–dipole interactions of 2,7-diaryl-TAPs were investigated by DFT calculations (Figures 5 and S16).[6−8] As a comparable skeleton, bis(4-tolyl)-TAP (**5aa**) has a dipole moment (5.1 D) with the almost same direction along the substituent at C7-position. The direction of the substituent at C2-position is almost orthogonal to that at C7-position. The donor or acceptor units at C2-position may change the direction of the total dipole moment. Compared with **5aa**, **5ad** (**A** ring = 4-tolyl; **B** ring = 4-dimethylaminophenyl) exhibits a larger dipole moment (8.0 D), and **5af** (**A** ring = 4-tolyl; **B** ring = 3,5-bis(trifluoromethyl)-phenyl) has a smaller dipole moment (1.3 D), indicating that an EDG on 7-aryl may enhance the dipole moment, while an EWG on 7-aryl may cancel the intrinsic dipole moment. However, **5da** (**A** ring = 4-dimethylaminophenyl; **B** ring = 4-tolyl) shows a dipole moment (4.7 D) similar to that of **5aa**, and **5fa** (**A** ring = 3,5-bis(trifluoromethyl)phenyl; **B** ring = 4-tolyl) exhibits a larger dipole moment (7.7 D) than **5aa**, suggesting that an EDG on 2-aryl may have a small influence on the electric dipole moment, while an EWG on 2-aryl may enhance the intrinsic dipole moment. Consistent with these trends, the dipole moments of **5df** and **5fd** were evaluated to be 2.4 and 10.4 D by DFT calculations, respectively.

Given that the strong face-to-face $\pi-\pi$ and dipole–dipole interactions enable to compensate the torsional tension,[17] the **B-TAP** section of 2,7-diaryl-TAPs may adopt a more planar geometry. Thus, a large molecular dipole moment of **5fd** triggers a cross-parallel packing arrangement in the crystals, in which the dihedral angles of the **A** and **B** rings with the TAP core converge to render a roughly coplanar conformation (Figure 4c). The external stimuli can enable to destroy the molecular planarity of **5fd** and weaken intermolecular $\pi-\pi$ interactions, thus leads to a blue-shifted emission. For **5df**, the

DOI: 10.1021/jacs.6b03890
J. Am. Chem. Soc. 2016, 138, 12803−12812

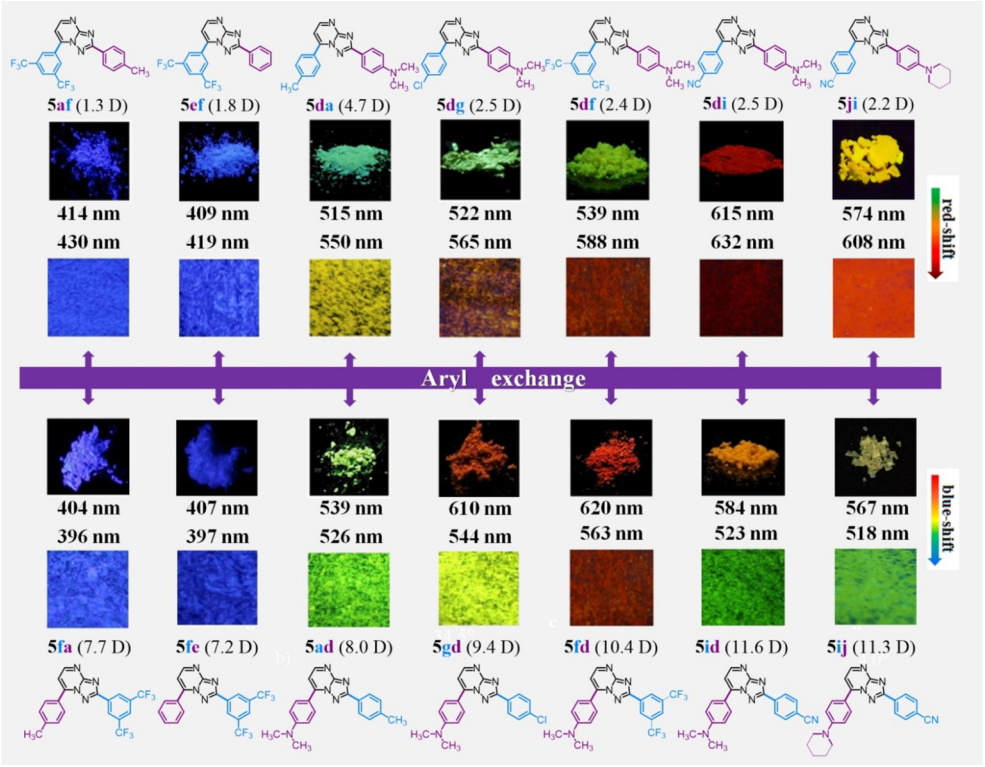

Figure 5. Calculated dipole moments of 2,7-diaryl-TAPs and their fluorescent images before and after grinding.

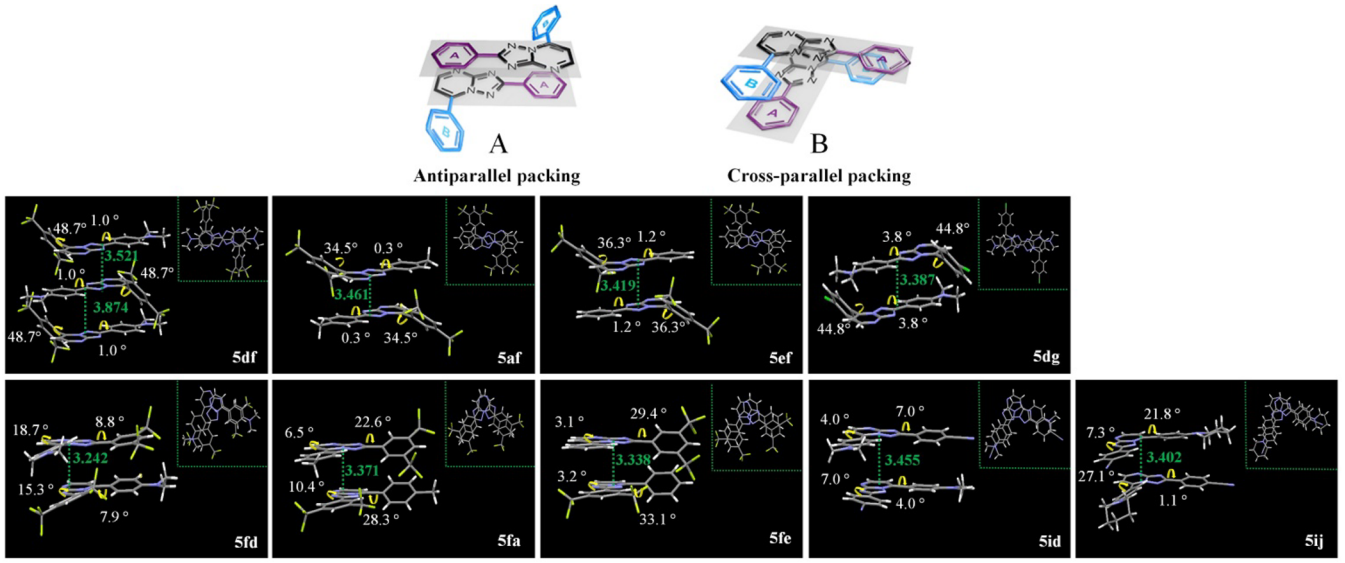

Figure 6. Packing modes of crystals of 2,7-diaryl-TAPs. The top view of the crystalline packing is shown in the upper right corner. (Top) antiparallel packing mode; (bottom) cross-parallel packing mode.

intermolecular dipole−dipole interactions cannot offer enough compensation for the torsional tension generated by the planarization of the twisted conformation due to a small dipole moment. Thus, **5df** adopts the antiparallel $\pi-\pi$ stacking mode through the overlap of **A-TAP** planes (Figure 4b). External force can induce conformation planarization of the twisted **B-TAP** segment and increase intermolecular $\pi-\pi$ stacking interactions, which is responsible for red-shifted emission. Thus, we conceive that the packing modes and mechanochromic trends of 2,7-diaryl-TAPs are greatly related to the dipole moment. Like **5df**, the other six red-shifted mechanochromic luminogens (**5af**, **5ef**, **5da**, **5dg**, **5di**, and **5ji**) have relatively small dipole moments. Similar to **5fd**, their isomers (**5fa**, **5fe**, **5ad**, **5gd**, **5id**, and **5ij**) with blue-shifted mechanochromism exhibit relatively large dipole moments (Figure 5).

Fortunately, in addition to **5df** and **5fd** mentioned above, we obtained other seven single crystals of 2,7-diaryl-TAPs (**5af**, **5ef**, **5dg**, **5fa**, **5fe**, **5id**, and **5ij**) by slow diffusion of hexane or petroleum ether vapor into a solution of 2,7-diaryl-TAP in dichloromethane or chloroform at 20 °C. The single-crystal XRD analysis discloses that **5af**, **5ef**, and **5dg** take the antiparallel fashion similar to **5df**, and **5fa**, **5fe**, **5id**, and **5ij**

DOI: 10.1021/jacs.6b03890
J. Am. Chem. Soc. 2016, 138, 12803−12812

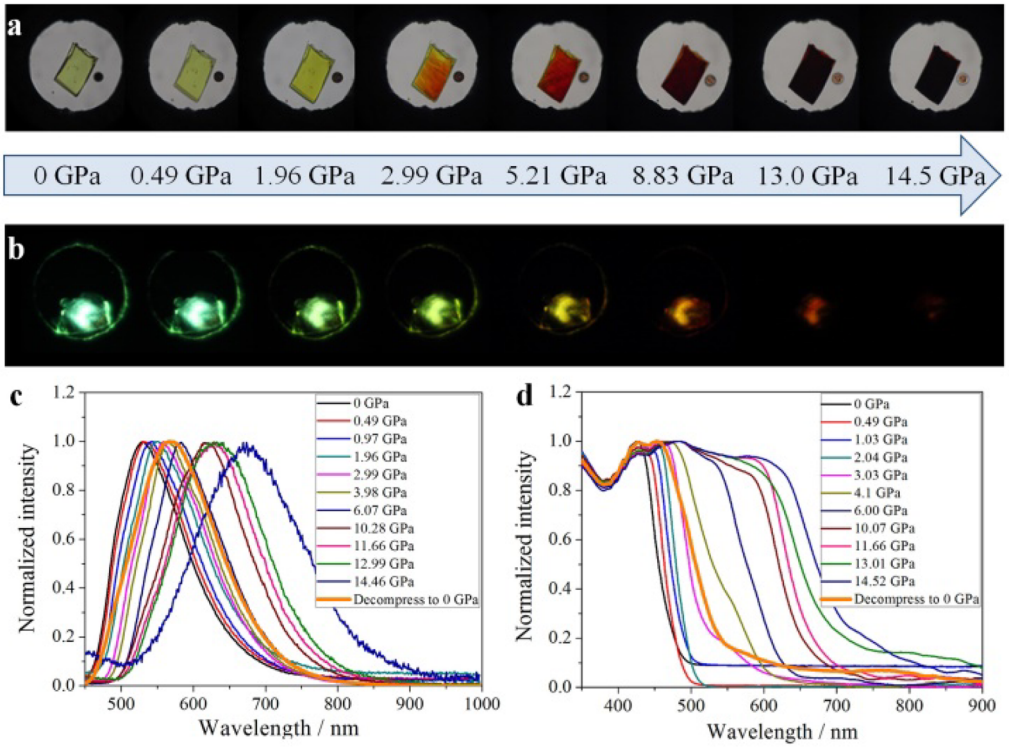

Figure 7. Visible (a) and fluorescent (b) micrographs of single-crystalline **5df** under different pressures. Emission (c) and absorption (d) spectra of single-crystalline **5df** under different pressures.

tend to adopt the cross-parallel packing mode like **5fd** (Figure 6). It is worth noting that **5df** and **5fd**, **5af** and **5fa**, and **5ef** and **5fe** are three pairs of isomers with the interchanged **A** and **B** rings, which could provide further support to understand the relationship between molecular structure and mechanochromic luminescent behavior.

Mechanochromic Properties Using Silicone Oil and Argon as the Pressure-Transmitting Media. The mechanochromic behaviors of a single-crystalline specimen of **5df** were first investigated using silicone oil as a pressure-transmitting medium. The high-pressure experiments were performed by using a diamond anvil cell, and pressures were applied up to 14.5 GPa in silicone oil as the pressure-transmitting medium. The visible and fluorescent images of **5df** as well as the absorption and emission spectra under different pressures are shown in Figure 7. To our delight, the single-crystalline **5df** also shows a red-shifted emission in silicone oil, which is more significant than that upon grinding. As the pressure increases to 14.5 GPa, the single-crystalline specimen exhibits a color change from green (λ_{em} = 524 nm) to deep red (λ_{em} = 676 nm), which is one of the largest mechanochromic shifts (152 nm) reported to date.[3,11,21,43,46] Under 6.07 GPa, the emission shifts to 585 nm similar to that of the powder after grinding (Figure S8), indicating that grinding is not powerful enough to give rise to a stronger mechanochromic effect. With the increase of the applied pressure, the absorption peaks broaden with the formation of two new peaks at 483 and 581 nm. The change trends of both the emission and absorption of the single-crystalline specimen in silicone oil are similar to those under grinding, implying the similar mechanochromic mechanism under different mechanical stimuli. It is worthy of note that the fluorescence and absorption spectra cannot entirely restore to the original state after releasing the pressure (from 14.5 to 0 GPa) (Figures 7 and S12a,b). In addition, we also performed the high-pressure experiments using argon as the pressure-transmitting medium. The same change trends of both the emission and absorption of the single-crystalline specimen were observed in these two pressure-transmitting media (Figure S12c–f).

Practical Applications. The further practical applications of these mechanochromic materials are illustrated in Figure 8. The powder of **5df** dispersed on a filter paper as a thin-film exhibited a yellow-green emission upon excitation by UV lamp (λ_{ex} = 365 nm). Then, the letters "TAP" were written on the thin-film with a spatula as a "pen". Due to the writing-induced

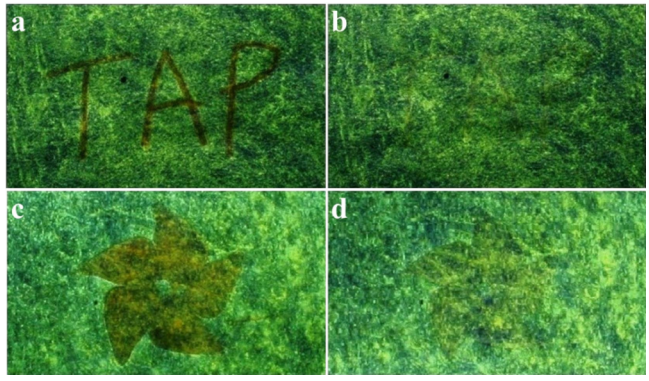

Figure 8. Mechanochromic application and relationship between mechanical pressure and emission maximum. Photographs a–d are shown under UV light (365 nm). (a) Letters "TAP" were written on **5df**-coated filter paper using a spatula. (b) The letters were erased after treating the coating paper in CH_2Cl_2 vapor. (c) A pattern of flower was printed on **5df**-coated filter paper under mechanical pressure. (d) The pattern became invisible after treating the coating paper by thermal annealing.

DOI: 10.1021/jacs.6b03890
J. Am. Chem. Soc. 2016, 138, 12803–12812

mechanochromism, the letters emitted an orange-red fluorescence (Figure 8a). These letters could be easily erased by using CH_2Cl_2 vapor as an "eraser" or heating at 120 °C for 5 min (Figure 8b). Next, an orange flower was printed on the yellow-green-emitting paper under pressure (Figure 8c), and the printed flower could be erased by heating at 120 °C for 5 min to restore the original emission color (Figure 8d). Further investigation demonstrates an approximately linear correlation between the mechanical pressure and the mechanochromic performance of **5df** with respect to the peak wavelengths (Figure S13). These results illustrate that the rewritable information storage systems could be constructed if we judiciously utilize the characteristics of the reversible chromism.

CONCLUSIONS

In summary, a novel strategy for the design of mechanochromic luminogens has been presented, based on the dipole moment of D-A molecules, exemplified by 2,7-diaryl-TAPs. The programmed C−H arylation provides a straightforward gateway toward 2,7-diaryl-TAPs, which unlocks an opportunity to rapidly assemble a library of D-A-type luminogens and to better understand their structure−property relationships. Molecular dipole moment has been employed to explain and further predict the mechanochromic trends. 2,7-Diaryl-TAPs with EDGs on the 2-aryl and EWGs on the 7-aryl exhibit a red-shifted mechanochromic trend. When the two aryls are interchanged, the resulting luminogens exhibit a blue-shifted mechanochromism. Finally, seven pairs of aryl-interchanged congeners with opposite mechanochromic trends have been obtained through a rational molecular design. When silicone oil is used as the pressure-transmitting medium, **5df** shows a significant red shift of 152 nm in emission wavelength, which is one of the largest mechanochromic shifts reported, to date. The design principle of mechanochromic luminogens developed herein should inspire the development of novel mechanochromic materials.

ASSOCIATED CONTENT

Supporting Information

The Supporting Information is available free of charge on the ACS Publications website at DOI: 10.1021/jacs.6b03890.

Detailed information on experimental procedures; computational, crystallographic, and spectroscopic data, including Figures S1−S16 and Tables S1−S5 (PDF)
X-ray crystal structure of **3d** (CCDC-1009530) (CIF)
X-ray crystal structure of **3e′** (CCDC-1009642) (CIF)
X-ray crystal structure of **4a** (CCDC-1009643) (CIF)
X-ray crystal structure of **5af** (CCDC-1035081) (CIF)
X-ray crystal structure of **5df** (CCDC-1009644) (CIF)
X-ray crystal structure of **5dg** (CCDC-1009542) (CIF)
X-ray crystal structure of **5fd** (CCDC-1009645) (CIF)
X-ray crystal structure of **5id** (CCDC-1009657) (CIF)
X-ray crystal structure of **5ef** (CCDC-1009534) (CIF)
X-ray crystal structure of **5fa** (CCDC-1493853) (CIF)
X-ray crystal structure of **5fe** (CCDC-1504574) (CIF)
X-ray crystal structure of **5ij** (CCDC-1495696) (CIF)

AUTHOR INFORMATION

Corresponding Authors

*jingbolan@scu.edu.cn
*zoubo@jlu.edu.cn
*jsyou@scu.edu.cn

Author Contributions

§J.W. and Y.C. contributed equally to this work.

Notes

The authors declare no competing financial interest.

ACKNOWLEDGMENTS

The authors acknowledge the National NSF of China (Nos. 21432005, 21372164, 21321061, and 91227202) and Sichuan Provincial Foundation (2012JQ0002) for financial support.

REFERENCES

(1) Sagara, Y.; Kato, T. *Nat. Chem.* **2009**, *1*, 605.
(2) Davis, D. A.; Hamilton, A.; Yang, J.; Cremar, L. D.; Gough, D. V.; Potisek, S. L.; Ong, M. T.; Braun, P. V.; Martínez, T. J.; White, S. R.; Moore, J. S.; Sottos, N. R. *Nature* **2009**, *459*, 68.
(3) Sagara, Y.; Yamane, S.; Mitani, M.; Weder, C.; Kato, T. *Adv. Mater.* **2016**, *28*, 1073.
(4) Ito, H.; Muromoto, M.; Kurenuma, S.; Ishizaka, S.; Kitamura, N.; Sato, H.; Seki, T. *Nat. Commun.* **2013**, *4*, 2009.
(5) Sun, H.; Liu, S.; Lin, W.; Zhang, K. Y.; Lv, W.; Huang, X.; Huo, F.; Yang, H.; Jenkins, G.; Zhao, Q.; Huang, W. *Nat. Commun.* **2014**, *5*, 3601.
(6) Yagai, S.; Okamura, S.; Nakano, Y.; Yamauchi, M.; Kishikawa, K.; Karatsu, T.; Kitamura, A.; Ueno, A.; Kuzuhara, D.; Yamada, H.; Seki, T.; Ito, H. *Nat. Commun.* **2014**, *5*, 4013.
(7) Zhang, G.; Lu, J.; Sabat, M.; Fraser, C. L. *J. Am. Chem. Soc.* **2010**, *132*, 2160.
(8) Yoon, S.-J.; Chung, J. W.; Gierschner, J.; Kim, K. S.; Choi, M.-G.; Kim, D.; Park, S. Y. *J. Am. Chem. Soc.* **2010**, *132*, 13675.
(9) Luo, X.; Li, J.; Li, C.; Heng, L.; Dong, Y. Q.; Liu, Z.; Bo, Z.; Tang, B. Z. *Adv. Mater.* **2011**, *23*, 3261.
(10) Yuan, W. Z.; Tan, Y.; Gong, Y.; Lu, P.; Lam, J. W. Y.; Shen, X. Y.; Feng, C.; Sung, H. H-Y.; Lu, Y.; Williams, I. D.; Sun, J. Z.; Zhang, Y.; Tang, B. Z. *Adv. Mater.* **2013**, *25*, 2837.
(11) Dong, Y.; Xu, B.; Zhang, J.; Tan, X.; Wang, L.; Chen, J.; Lv, H.; Wen, S.; Li, B.; Ye, L.; Zou, B.; Tian, W. *Angew. Chem., Int. Ed.* **2012**, *51*, 10782.
(12) Teng, M.-J.; Jia, X.-R.; Chen, X.-F.; Wei, Y. *Angew. Chem., Int. Ed.* **2012**, *51*, 6398.
(13) Zhao, D.; Li, G.; Wu, D.; Qin, X.; Neuhaus, P.; Cheng, Y.; Yang, S.; Lu, Z.; Pu, X.; Long, C.; You, J. *Angew. Chem., Int. Ed.* **2013**, *52*, 13676.
(14) Nagura, K.; Saito, S.; Yusa, H.; Yamawaki, H.; Fujihisa, H.; Sato, H.; Shimoikeda, Y.; Yamaguchi, S. *J. Am. Chem. Soc.* **2013**, *135*, 10322.
(15) Li, G.; Song, F.; Wu, D.; Lan, J.; Liu, X.; Wu, J.; Yang, S.; Xiao, D.; You, J. *Adv. Funct. Mater.* **2014**, *24*, 747.
(16) Galer, P.; Korošec, R. C.; Vidmar, M.; Šket, B. *J. Am. Chem. Soc.* **2014**, *136*, 7383.
(17) Wang, L.; Wang, K.; Zou, B.; Ye, K.; Zhang, H.; Wang, Y. *Adv. Mater.* **2015**, *27*, 2918.
(18) Mao, Z.; Yang, Z.; Mu, Y.; Zhang, Y.; Wang, Y.-F.; Chi, Z.; Lo, C.-C.; Liu, S.; Lien, A.; Xu, J. *Angew. Chem., Int. Ed.* **2015**, *54*, 6270.
(19) Mutai, T.; Satou, H.; Araki, K. *Nat. Mater.* **2005**, *4*, 685.
(20) Varghese, S.; Das, S. *J. Phys. Chem. Lett.* **2011**, *2*, 863.
(21) Chi, Z.; Zhang, X.; Xu, B.; Zhou, X.; Ma, C.; Zhang, Y.; Liu, S.; Xu, J. *Chem. Soc. Rev.* **2012**, *41*, 3878.
(22) Hunter, C. A.; Sanders, J. K. M. *J. Am. Chem. Soc.* **1990**, *112*, 5525.
(23) Janiak, C. *J. Chem. Soc., Dalton Trans.* **2000**, 3885.
(24) Liu, X.; Xu, Z.; Cole, J. M. *J. Phys. Chem. C* **2013**, *117*, 16584.
(25) Grabowski, Z. R.; Rotkiewicz, K.; Rettig, W. *Chem. Rev.* **2003**, *103*, 3899.
(26) Dahlgren, M. K.; Schyman, P.; Tirado-Rives, J.; Jorgensen, W. L. *J. Chem. Inf. Model.* **2013**, *53*, 1191.
(27) Zhang, Y.; Sun, J.; Zhuang, G.; Ouyang, M.; Yu, Z.; Cao, F.; Pan, G.; Tang, P.; Zhang, C.; Ma, Y. *J. Mater. Chem. C* **2014**, *2*, 195.
(28) Kamala, K.; Rao, P. J.; Reddy, K. K. *Bull. Chem. Soc. Jpn.* **1988**, *61*, 3791.

DOI: 10.1021/jacs.6b03890
J. Am. Chem. Soc. 2016, 138, 12803−12812

(29) Salgado, A.; Varela, C.; Collazo, A. M. G.; García, F.; Pevarello, P.; Alkorta, I.; Elguero, J. *J. Mol. Struct.* **2011**, *987*, 13.
(30) Petrich, S. A.; Qian, Z.; Santiago, L. M.; Gupton, J. T.; Sikorski, J. A. *Tetrahedron* **1994**, *50*, 12113.
(31) Alberico, D.; Scott, M. E.; Lautens, M. *Chem. Rev.* **2007**, *107*, 174.
(32) Wencel-Delord, J.; Glorius, F. *Nat. Chem.* **2013**, *5*, 369.
(33) Segawa, Y.; Maekawa, T.; Itami, K. *Angew. Chem., Int. Ed.* **2015**, *54*, 66.
(34) Kim, E.; Koh, M.; Lim, B. J.; Park, S. B. *J. Am. Chem. Soc.* **2011**, *133*, 6642.
(35) Ma, Z.; Sun, W.; Himmelberger, S.; Vandewal, K.; Tang, Z.; Bergqvist, J.; Salleo, A.; Andreasen, J. W.; Inganäs, O.; Andersson, M. R.; Müller, C.; Zhang, F.; Wang, E. *Energy Environ. Sci.* **2014**, *7*, 361.
(36) Sekita, M.; Jiménez, Á. J.; Marcos, M. L.; Caballero, E.; Rodríguez-Morgade, M. S.; Guldi, D. M.; Torres, T. *Chem. - Eur. J.* **2015**, *21*, 19028.
(37) Li, D.; Zhang, H.; Wang, C.; Huang, S.; Guo, J.; Wang, Y. *J. Mater. Chem.* **2012**, *22*, 4319.
(38) Hansch, C.; Leo, A.; Taft, R. W. *Chem. Rev.* **1991**, *91*, 165.
(39) Herbich, J.; Kapturkiewicz, A. *J. Am. Chem. Soc.* **1998**, *120*, 1014.
(40) Cheng, Y.; Li, G.; Liu, Y.; Shi, Y.; Gao, G.; Wu, D.; Lan, J.; You, J. *J. Am. Chem. Soc.* **2016**, *138*, 4730.
(41) Rao, R. M.; Liao, C.-W.; Sun, S.-S. *J. Mater. Chem. C* **2013**, *1*, 6386.
(42) Mallesham, G.; Swetha, C.; Niveditha, S.; Mohanty, M. E.; Babu, N. J.; Kumar, A.; Bhanuprakash, K.; Rao, V. J. *J. Mater. Chem. C* **2015**, *3*, 1208.
(43) Zhang, X.; Chi, Z.; Zhang, J.; Li, H.; Xu, B.; Li, X.; Liu, S.; Zhang, Y.; Xu, J. *J. Phys. Chem. B* **2011**, *115*, 7606.
(44) Jenekhe, S. A.; Osaheni, J. A. *Science* **1994**, *265*, 765.
(45) Tanaka, J.; Koda, T.; Shionoya, S.; Minomura, S. *Bull. Chem. Soc. Jpn.* **1965**, *38*, 1559.
(46) Mitchell, D. J.; Schuster, G. B.; Drickamer, H. G. *J. Am. Chem. Soc.* **1977**, *99*, 1145.

DOI: 10.1021/jacs.6b03890
J. Am. Chem. Soc. 2016, 138, 12803−12812